# Solar wind proton temperature anisotropy: Linear theory and WIND/SWE observations

Petr Hellinger,[1] Pavel Trávníček,[1] Justin C. Kasper,[2] and Alan J. Lazarus[2]

Received 1 February 2006; revised 13 March 2006; accepted 29 March 2006; published 6 May 2006.

[1] We present a comparison between WIND/SWE observations (Kasper et al., 2006) of $\beta_{\|p}$ and $T_{\perp p}/T_{\|p}$ (where $\beta_{\|p}$ is the proton parallel beta and $T_{\perp p}$ and $T_{\|p}$ are the perpendicular and parallel proton temperatures, respectively; here parallel and perpendicular indicate directions with respect to the ambient magnetic field) and predictions of the Vlasov linear theory. In the slow solar wind, the observed proton temperature anisotropy seems to be constrained by oblique instabilities, by the mirror one and the oblique fire hose, contrary to the results of the linear theory which predicts a dominance of the proton cyclotron instability and the parallel fire hose. The fast solar wind core protons exhibit an anticorrelation between $\beta_{\|c}$ and $T_{\perp c}/T_{\|c}$ (where $\beta_{\|c}$ is the core proton parallel beta and $T_{\perp c}$ and $T_{\|c}$ are the perpendicular and parallel core proton temperatures, respectively) similar to that observed in the HELIOS data (Marsch et al., 2004). **Citation:** Hellinger, P., P. Trávníček, J. C. Kasper, and A. J. Lazarus (2006), Solar wind proton temperature anisotropy: Linear theory and WIND/SWE observations, *Geophys. Res. Lett.*, *33*, L09101, doi:10.1029/2006GL025925.

## 1. Introduction

[2] Thermalization due to Coulomb relaxation in the solar wind is generally insufficient to account for how closely particle distribution functions resemble to Maxwellian ones. Departures from the Maxwellian particle distribution functions are a possible source of free energy for many different instabilities. As a feed-back, the instabilities constrain the shape of particle distribution functions. In this letter we investigate threshold conditions of instabilities driven by proton temperature anisotropies:

[3] In the case of the proton temperature anisotropy $T_{\perp p} > T_{\|p}$ (for symbol definitions, see appendix A) the relevant instabilities are the proton cyclotron [e.g., *Gary et al.*, 1994] and the mirror modes [e.g., *Pokhotelov et al.*, 2004, and references therein]. The approximate threshold conditions $\gamma_{\max} \sim 0$ for the two instabilities may be fitted by an analytic relation

$$\frac{T_{\perp p}}{T_{\|p}} = 1 + \frac{a}{\beta_{\|p}^{b}} \tag{1}$$

where $a$ and $b$ are the fitted parameters. *Samsonov et al.* [2001] give the following fitted parameters of equation (1) for $\gamma_{\max} = 10^{-3}\ \omega_{cp}$: $a \simeq 0.45$ and $b \simeq 0.40$ for the proton cyclotron instability and $a \simeq 0.74$ and $b \simeq 0.73$ for the mirror instability. Activity associated with the proton cyclotron instability has been reported in ACE observations by *Gary et al.* [2001] in the fast solar wind and in Wind observations by *Kasper et al.* [2003] in the slow solar wind. However, in the fast solar wind the proton distributions often contain a core and a beam [*Marsch et al.*, 1982] and in the HELIOS observations by *Marsch et al.* [2004] the core protons in the fast solar wind ($v_{sw} > 600$ km/s) did not appear to be constrained by the proton cyclotron threshold condition calculated for the core protons (which are assumed bi-Maxwellian and the proton beam population is neglected); however, the whole proton core-beam distribution function may become unstable with respect to the proton cyclotron instability [*Marsch*, 1991].

[4] *Marsch et al.* [2004] showed that the core protons exhibit an anticorrelation between anisotropy and beta in the following form

$$\frac{T_{\perp c}}{T_{\|c}} \sim \frac{a}{\beta_{\|c}^{b}} \tag{2}$$

with $a \simeq 1.16$ and $b \simeq 0.55$. This relation (constraint) is not well understood. Also, the role of the mirror instability in the slow solar wind remains unclear [*Kasper et al.*, 2003].

[5] In the case of the proton temperature anisotropy $T_{\perp p} < T_{\|p}$ the relevant instabilities are the parallel fire hose [*Quest and Shapiro*, 1996; *Farrugia et al.*, 1998] and the oblique fire hose [*Hellinger and Matsumoto*, 2000]. *Gary et al.* [1998] showed that the approximate threshold conditions for the parallel fire hose may be given in the same form as in equation (1) but with $a < 0$: for $\gamma_{\max} = 10^{-3}\ \omega_{cp}$ they give the values $a \simeq -0.66$ and $b \simeq 0.56$. The observations of *Kasper et al.* [2002] demonstrated the existence of a limit to $T_{\perp p}/T_{\|p}$ due to the fire hose instability. However, that investigation compared fluid and kinetic calculations of the parallel fire hose, and did not consider the effect of the oblique fire hose.

[6] In this letter we extend the work of *Kasper et al.* [2002, 2003] by comparing the statistically large data set of the Wind/SWE solar wind data from 1995–2001 with the linear predictions for all four of the instabilities driven by the proton temperature anisotropy. The letter is organized as follows: in section 2 we briefly describe results of Vlasov linear theory and we give new fitted threshold conditions for the four instabilities. In section 3 we present the WIND/SWE data in the case of the slow and fast solar wind and

[1] Institute of Atmospheric Physics, Academy of Sciences of the Czech Republic, Prague, Czech Republic.
[2] Kavli Institute for Astrophysics and Space Research, Massachusetts Institute of Technology, Cambridge, Massachusetts, USA.


0094-8276/06/2006GL025925$05.00

**Table 1.** Fitted Parameters for Equation (3) for the Approximate Threshold Condition $\gamma_{max} = 10^{-3}$[a]

| Instability | $a$ | $b$ | $\beta_0$ |
|---|---|---|---|
| Proton cyclotron instability | 0.43 | 0.42 | −0.0004 |
| Mirror instability | 0.77 | 0.76 | −0.016 |
| Parallel fire hose | −0.47 | 0.53 | 0.59 |
| Oblique fire hose | −1.4 | 1.0 | −0.11 |

[a] $0.01 \le \beta_{\|p} \le 30$, $0.1 \le T_{\perp p}/T_{\|p} \le 10$; $\beta_e = 1$, $\omega_{pe}/\omega_{ce} = 100$.

compare them with the predictions of the linear theory. In section 4 we discuss the results.

## 2. Linear Theory

[7] In this section, we investigate the proton cyclotron, mirror, and parallel and oblique fire hose instabilities in a plasma consisting of protons and electrons. The plasma is assumed weakly magnetized $\omega_{pe}/\omega_{ce} = 100$, consisting of Maxwellian electrons with $\beta_e = 1$ and bi-Maxwellian protons. We calculated the maximum growth rate of the four instabilities in the region $0.01 < \beta_{\|p} < 30$ and $0.1 < T_{\perp p}/T_{\|p} < 10$. The relation $\gamma = 10^{-3}\omega_{cp}$ was than fitted for the four instabilities in the following, generalized form of equation (1):

$$\frac{T_{\perp p}}{T_{\|p}} = 1 + \frac{a}{\left(\beta_{\|p} - \beta_0\right)^b} \tag{3}$$

where $a$, $b$, and $\beta_0$ are the fitted parameters. The results of the fitting are summarized in Table 1. Table 1 gives the triads $a$, $b$, $\beta_0$ for the four instabilities. It shows that in the case of the proton cyclotron and mirror instabilities the approximation of equation (1) is reasonable: $\beta_0 \sim 0$ and the fitted parameters $a$ and $b$ are similar to those of *Samsonov et al.* [2001]. However, in the case of the fire hose instabilities the inclusion of $\beta_0$ term is important.

## 3. Observations

[8] Following *Kasper et al.* [2002], we use fitted data from the two Faraday Cup instruments in the Solar Wind Experiment (SWE) on the Wind spacecraft. WIND is a rotating spacecraft with a spin-axis perpendicular to the ecliptic plane and a period of three seconds. A Faraday Cup is an energy/charge instrument with a large, conical field of view which measures the current produced by particles within a given energy window. The proton density and the parallel and perpendicular proton temperatures are obtained using a non-linear least-squares fitting of data to a theoretical model assuming a bi-Maxwellian proton distribution function and the magnetic field direction obtained from three-second measurements provided by the Magnetic Field Investigation (MFI) on the Wind spacecraft. The fitting procedure separates contributions of core protons from alpha particles (and/or a proton beam) and gives a good estimate of core proton parallel and perpendicular temperatures accurate to approximately 8% [*Kasper et al.*, 2006].

### 3.1. Slow Solar Wind

[9] We start with the WIND/SWE data in the case of the slow solar wind. The results of the period 1995–2001 are given in Figure 1. Figure 1 shows a color scale plot of the relative observation frequency of $(\beta_{\|p}, T_{\perp p}/T_{\|p})$ in the fitted SWE data for the solar wind with $v_{sw} \le 600$ km/s [cf. *Kasper et al.*, 2002, Figure 2]. Note that we assume that there are no proton beam populations, setting $\beta_{\|c} = \beta_{\|p}$, $T_{\perp c} = T_{\perp p}$ and $T_{\|c} = T_{\|p}$. The (logarithmic) color scale is given on the right. The overplotted curves show the contours of the maximum growth rate $\gamma_{max}$ in the corresponding plasma with Maxwellian electrons and bi-Maxwellian protons with $\beta_{\|p}$ and $T_{\perp p}/T_{\|p}$; other plasma parameters are given in Table 1. Figure 1 (left) displays the contours of $\gamma_{max}$ for the proton cyclotron instability (solid curves) and the parallel fire hose (dashed curves) whereas Figure 1 (right) displays the contours of $\gamma_{max}$ for the mirror instability (dotted curves) and the oblique fire hose (dash-dotted curves). The maximum growth rate is given in units of $\omega_{cp}$. Note that the two contours $10^{-3}$ and $10^{-2}$ of the maximum growth rate for the oblique fire hose are indistinguishable on this scale.

[10] Figure 1 shows that a majority of observations lies outside the regions unstable with respect to the four instabilities (for the used plasma parameters). It also indicate two possible constraints for the higher $\beta_{\|p}$: one for $T_{\perp p}/T_{\|p} > 1$ and another for $T_{\perp p}/T_{\|p} < 1$ [cf. *Kasper et al.*, 2006]. For $T_{\perp p} > T_{\|p}$ the apparent constraint is compatible with the threshold condition for the mirror instability. The linear predictions for parallel proton cyclotron instability does not seem to constrain the observations. For $T_{\perp p} < T_{\|p}$ the constraint seems to be more compatible with the oblique fire hose than with the parallel one, at least for $\beta_{\|p} \gtrsim 2$.

### 3.2. Fast Solar Wind

[11] Now we continue with the WIND/SWE data in the case of the fast solar wind. The results of the period 1995–2001 are given in Figure 2 which has the same format as Figure 1. Figure 2 shows a color scale plot of the relative

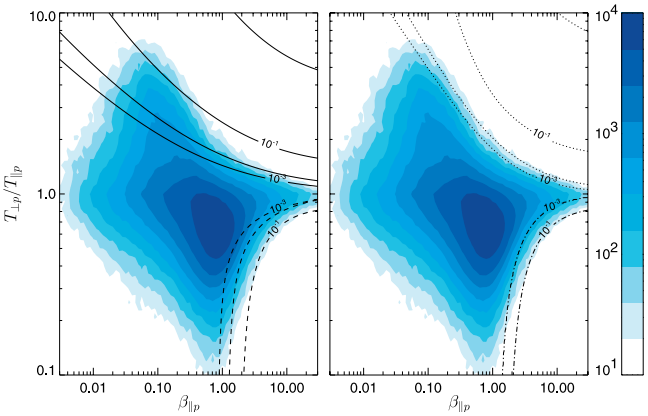


**Figure 1.** A color scale plot of the relative frequency of $(\beta_{\|p}, T_{\perp p}/T_{\|p})$ in the WIND/SWE data (1995–2001) for the solar wind with $v_{sw} \le 600$ km/s [cf. *Kasper et al.*, 2002, Figure 2]. The (logarithmic) color scale is show on the right. The over plotted curves show the contours of the maximum growth rate (in units of $\omega_{cp}$) in the corresponding bi-Maxwellian plasma (left) for the proton cyclotron instability (solid curves) and the parallel fire hose (dashed curves) and (right) for the mirror instability (dotted curves) and the oblique fire hose (dash-dotted curves).

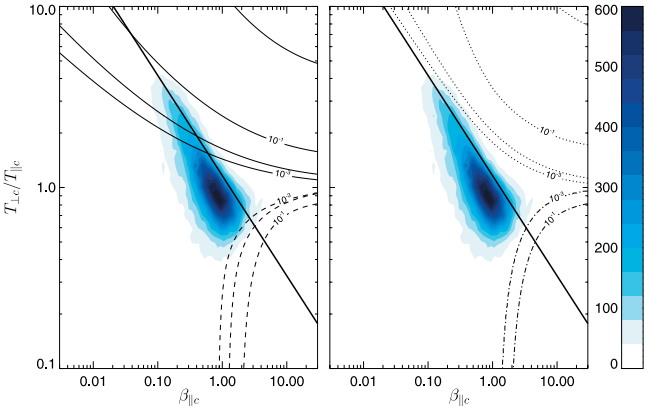


**Figure 2.** A color scale plot of the relative frequency of ($\beta_{\|c}$, $T_{\perp c}/T_{\|c}$) in the WIND/SWE data (1995–2001) for the solar wind with $v_{sw} > 600$ km/s. The color scale is show on the right. The over plotted curves show the contours of the maximum growth rate (in units of $\omega_{cp}$) in the corresponding plasma (left) for the proton cyclotron instability (solid curves) and the parallel fire hose (dashed curves) and (right) for the mirror instability (dotted curves) and the oblique fire hose (dash-dotted curves). The dash-dot-dot-dotted lines denote equation (2) between $T_{\perp c}/T_{\|c}$ and $\beta_{\|c}$ found in the HELIOS data [*Marsch et al.*, 2004].

frequency of ($\beta_{\|c}$, $T_{\perp c}/T_{\|c}$) in the fitted SWE data for the solar wind with $v_{sw} > 600$ km/s. The overplotted curves show the contours of $\gamma_{max}$ in the corresponding plasma with Maxwellian electrons and bi-Maxwellian protons with $\beta_{\|p} = \beta_{\|c}$ and $T_{\perp p}/T_{\|p} = T_{\perp c}/T_{\|c}$; the other plasma parameters are given in Table 1. Figure 2 (left) displays $\gamma_{max}$ for the proton cyclotron instability (solid curves) and the parallel fire hose (dashed curves), whereas Figure 2 (right) displays $\gamma_{max}$ for the mirror instability (dotted curves) and the oblique fire hose (dash-dotted curves). The dash-dot-dot-dotted lines denote equation (2) between the parameters $T_{\perp c}/T_{\|c}$ and $\beta_{\|c}$ of the core protons found in the HELIOS data [*Marsch et al.*, 2004].

[12] Similar to the case of the slow solar wind, Figure 2 shows that a majority of observations lies outside the regions unstable with respect to the four instabilities (for the used plasma parameters). The data shows a clear anticorrelation between $\beta_{\|c}$ and $T_{\perp c}/T_{\|c}$ which is similar to that observed by *Marsch et al.* [2004]. For $T_{\perp c}/T_{\|c} > 1$ the observations seems to be only weakly constrained by the mirror instability (but not by the proton cyclotron instability) whereas the parallel proton fire hose may be responsible for the constraint in the case of $T_{\perp c}/T_{\|c} < 1$.

## 4. Discussion

[13] We have presented a comparison between the statistically large data set of the WIND/SWE Faraday Cup observations [*Kasper et al.*, 2006] of the proton parameters $\beta_{\|c}$ and $T_{\perp c}/T_{\|c}$ and $\beta_{\|p}$ and $T_{\perp p}/T_{\|p}$ (assumed in the case of the slow solar wind) and the predictions of the Vlasov linear theory. The linear theory (for the plasma consisting of Maxwellian electrons and bi-Maxwellian protons) predicts four distinct instabilities: proton cyclotron, mirror, parallel and oblique fire hose instabilities. Their approximate threshold conditions may be given in the form of equation (3) with the fitted parameters $a$, $b$ and $\beta_0$ shown in Table 1. The parameter $\beta_0$ in equation (3) is important only for the two fire hose instabilities; for the proton cyclotron and mirror instabilities we recover the previous results, equation (1) [cf. *Samsonov et al.*, 2001].

[14] In the slow solar wind, the observed proton temperature anisotropy seems to be constrained by the oblique instabilities (the mirror one and oblique fire hose). This result is in contradiction with the results of the linear theory which predicts that the proton cyclotron instability and of the parallel fire hose would dominate for all but large proton betas, $\beta_{\|p}$ 10. The fast solar wind core protons exhibit an anticorrelation between $\beta_{\|c}$ and $T_{\perp c}/T_{\|c}$ similar to that observed in the HELIOS data [*Marsch et al.*, 2004]. These observations also indicate a possible constraining role of the mirror and parallel fire hose instabilities. On the other hand, the observations by *Gary et al.* [2001] show constraints consistent with the proton cyclotron instability based on the total proton parameters whereas we use the core proton parameters [cf. *Marsch et al.*, 2004].

[15] The disagreement between the predictions of the linear theory and the observations could be related to the assumed plasma composition and particle distribution functions. Indeed, observed proton distribution functions exhibit departures from the bi-Maxwellian distribution function, especially in the fast solar wind [*Marsch et al.*, 1982]; also *Marsch and Tu* [2001] reported a quasi-linear cyclotron plateau-like proton distribution function. Moreover, for example a presence of non negligible abundance of alpha particles (and other plasma parameters as electron temperatures) influences all the four instabilities [*Dasso et al.*, 2003; *Gary et al.*, 2003; *Hellinger and Trávníèek*, 2006]. Another possible explanation of the disagreement could be related to nonlinear effects owing to the different linear and saturation properties of the instabilities. Hybrid simulations indicate [*McKean et al.*, 1992, 1994] that the mirror instability is more robust than the proton cyclotron one. Similarly, in the case of the competition between the parallel and oblique fire hose instabilities the latter is more robust than the former one [*Hellinger and Matsumoto*, 2001; *Hellinger et al.*, 2003]. The properties of proton temperature anisotropies obviously depend on mechanisms which drive them. Let us briefly discuss some of these mechanisms: The solar wind expansion is expected to drive $T_{\|p} > T_{\perp p}$ (at least for a nearly radial magnetic field). Numerical simulations [*Hellinger et al.*, 2003; *Matteini et al.*, 2005] show that an ideal expansion could drive the system relatively far inside the region unstable with respect to the parallel fire hose instability and to drive the oblique fire hose unstable. These may explain the observation results we present in this letter (however, these simulations assume non realistic expansion time scales). A natural driving mechanism for generation of $T_{\perp p} > T_{\|p}$ (and $T_{\perp c} > T_{\|c}$) is the proton cyclotron resonance with left-handed cyclotron waves [*Hollweg and Isenberg*, 2002]. The cyclotron resonance heating may lead to the anticorrelation, equation (2) [*Marsch et al.*, 2004]. Numerical simulations [*Hellinger et al.*, 2005] moreover show that the cyclotron resonance may drive minor ions unstable with respect to the corresponding

cyclotron instability. An equivalent effect may explain the apparent disagreement between the observations and linear theory for protons.

[16] Further theoretical, simulation, and observation work is needed to investigate role of different instabilities in the solar wind. It is important to include more realistic plasma compositions, a good description of the particle distribution functions and identification of active instabilities (e.g., in the magnetosheath context [*Lacombe and Belmont*, 1995]).

## Appendix A: Definitions

[17] We use subscripts $\perp$ and $\parallel$ to denote the directions with respect to the ambient magnetic field $\boldsymbol{B}_0$ with $B_0 = |\boldsymbol{B}_0|$ denoting its magnitude. Here $T_{\perp p}$ and $T_{\parallel p}$ are the perpendicular and parallel proton temperatures (with respect to $\boldsymbol{B}_0$), respectively, whereas $T_{\perp c}$ and $T_{\parallel c}$ denotes the perpendicular and parallel temperatures of core protons. respectively; $T_e$ denotes the (isotropic) electron temperature. We define $\beta_{\parallel p} = 2\mu_0 n_p k_B T_{\parallel p}/B_0^2$, $\beta_{\parallel c} = 2\mu_0 n_c k_B T_{\parallel c}/B_0^2$ and $\beta_e = 2\mu_0 n_e k_B T_e/B_0^2$. The proton and electron cyclotron frequency are $\omega_{cp} = eB_0/m_p$ and $\omega_{ce} = eB_0/m_e$, respectively, the electron plasma frequency is $\omega_{pe} = (ne^2/m_e\epsilon_0)^{1/2}$. In these expressions $m_p$ and $m_e$ denote the electron and proton mass, respectively, $n_e$ and $n_p$ are the electron and proton number densities, respectively, $n_c$ is the number density of core protons, $e$ is the proton charge, $\mu_0$ and $\epsilon_0$ stand for the vacuum magnetic permeability and electric permittivity, respectively, and $k_B$ is Boltzmann constant. Finally, we denote the maximum grow rate $\gamma_{\max}$ and the solar wind velocity $v_{sw}$.

[18] **Acknowledgment.** Authors acknowledge the Czech grant GA AV IAA3042403, ESA PECS 98024 and NASA grant NAG-10915, and thank A. Szabo from the WIND/MFI experiment for the magnetic field data.

## References

Dasso, S., F. T. Gratton, and C. J. Farrugia (2003), A parametric study of the influence of ion and electron properties on the excitation of electromagnetic ion cyclotron waves in coronal mass ejections, *J. Geophys. Res.*, *108*(A4), 1149, doi:10.1029/2002JA009558.

Farrugia, C. J., F. T. Gratton, G. Gnavi, and K. W. Ogilvie (1998), On the possible excitation of electromagnetic ion cyclotron waves in solar ejecta, *J. Geophys. Res.*, *103*, 6543–6550.

Gary, S. P., M. E. McKean, D. Winske, B. J. Anderson, R. E. Denton, and S. A. Fuselier (1994), The proton cyclotron instability and the anisotropy/β inverse correlation, *J. Geophys. Res.*, *99*, 5903–5914.

Gary, S. P., H. Li, S. O'Rourke, and D. Winske (1998), Proton resonant firehose instability: Temperature anisotropy and fluctuating field constraints, *J. Geophys. Res.*, *103*, 14,567–14,574.

Gary, S. P., R. M. Skoug, J. T. Steinberg, and C. W. Smith (2001), Proton temperature anisotropy constraint in the solar wind: ACE observations, *Geophys. Res. Lett.*, *28*, 2759–2763.

Gary, S. P., L. Yin, D. Winske, L. Ofman, B. E. Goldstein, and M. Neugebauer (2003), Consequences of proton and alpha anisotropies in the solar wind: Hybrid simulations, *J. Geophys. Res.*, *108*(A2), 1068, doi:10.1029/2002JA009654.

Hellinger, P., and H. Matsumoto (2000), New kinetic instability: Oblique Alfvén fire hose, *J. Geophys. Res.*, *105*, 10,519–10,526.

Hellinger, P., and H. Matsumoto (2001), Nonlinear competition between the Whistler and Alfvén fire hoses, *J. Geophys. Res.*, *106*, 13,215–13,218.

Hellinger, P., and P. Trávníček (2006), Parallel and oblique proton fire hose instabilities in the presence of alpha/proton drift: Hybrid simulations, *J. Geophys. Res.*, *111*, A01107, doi:10.1029/2005JA011318.

Hellinger, P., P. Trávníček, A. Mangeney, and R. Grappin (2003), Hybrid simulations of the expanding solar wind: Temperatures and drift velocities, *Geophys. Res. Lett.*, *30*(5), 1211, doi:10.1029/2002GL016409.

Hellinger, P., M. Velli, P. Trávníček, S. P. Gary, B. E. Goldstein, and P. C. Liewer (2005), Alfvén wave heating of heavy ions in the expanding solar wind: Hybrid simulations, *J. Geophys. Res.*, *110*, A12109, doi:10.1029/2005JA011244.

Hollweg, J. V., and P. A. Isenberg (2002), Generation of the fast solar wind: A review with emphasis on the resonant cyclotron interaction, *J. Geophys. Res.*, *107*(A7), 1147, doi:10.1029/2001JA000270.

Kasper, J. C., A. J. Lazarus, and S. P. Gary (2002), Wind/SWE observations of firehose constraint on solar wind proton temperature anisotropy, *Geophys. Res. Lett.*, *29*(17), 1839, doi:10.1029/2002GL015128.

Kasper, J. C., A. J. Lazarus, S. P. Gary, and A. Szabo (2003), Solar wind temperature anisotropies, in *Solar Wind Ten*, edited by M. Velli, R. Bruno, and F. Malara, *AIP Conf. Proc.*, *679*, 538–541.

Kasper, J., A. J. Lazarus, J. T. Steinberg, K. W. Ogilvie, and A. Szabo (2006), Physics-based tests to identify the accuracy of solar wind ion measurements: A case study with the Wind Faraday cups, *J. Geophys. Res.*, *111*, A03105, doi:10.1029/2005JA011442.

Lacombe, C., and G. Belmont (1995), Waves in the Earth's magnetosheath: Observations and interpretations, *Adv. Space Res.*, *15*, 329–340.

Marsch, E. (1991), Kinetic physics of the solar wind plasma, in *Physics of the Inner Heliosphere II: Particles, Waves and Turbulence, Physics and Chemistry in Space—Space and Solar Physics*, vol. 21, edited by R. Schwenn and E. Marsch, pp. 45–110, Springer, New York.

Marsch, E., and C.-Y. Tu (2001), Evidence for pitch angle diffusion of solar wind protons in resonance with cyclotron waves, *J. Geophys. Res.*, *106*, 8357–8362.

Marsch, E., K. H. Muhlhauser, R. Schwenn, H. Rosenbauer, W. Pilipp, and F. M. Neubauer (1982), Solar-wind protons: Three-dimensional velocity distributions and derived plasma parameters measured between 0.3 AU and 1 AU, *J. Geophys. Res.*, *87*, 52–72.

Marsch, E., X.-Z. Ao, and C.-Y. Tu (2004), On the temperature anisotropy of the core part of the proton velocity distribution function in the solar wind, *J. Geophys. Res.*, *109*, A04102, doi:10.1029/2003JA010330.

Matteini, L., S. Landi, P. Hellinger, and M. Velli (2005), Proton fire hose instability in the expanding solar wind, in *Proceedings of Solar Wind 11/SOHO 16*, vol. SP-592, edited by T. H. Zurbuchen and B. Fleck, pp. 503–506, Eur. Space Agency, Paris.

McKean, M. E., D. Winske, and S. P. Gary (1992), Kinetic properties of mirror waves in magnetosheath plasmas, *Geophys. Res. Lett.*, *19*, 1331–1334.

McKean, M. E., D. Winske, and S. P. Gary (1994), Two-dimensional simulations of ion anisotropy instabilities in the magnetosheath, *J. Geophys. Res.*, *99*, 11,141–11,153.

Pokhotelov, O. A., R. Z. Sagdeev, M. A. Balikhin, and R. A. Treumann (2004), Mirror instability at finite ion-larmor radius wavelengths, *J. Geophys. Res.*, *109*, A09213, doi:10.1029/2004JA010568.

Quest, K. B., and V. D. Shapiro (1996), Evolution of the fire-hose instability: Linear theory and wave-wave coupling, *J. Geophys. Res.*, *101*, 24,457–24,469.

Samsonov, A. A., M. I. Pudovkin, S. P. Gary, and D. Hubert (2001), Anisotropic MHD model of the dayside magnetosheath downstream of the oblique bow shock, *J. Geophys. Res.*, *106*, 21,689–21,700.

P. Hellinger and P. Trávníček, Institute of Atmospheric Physics, Academy of Sciences of the Czech Republic, Prague 14131, Czech Republic. (petr.hellinger@ufa.cas.cz; trav@ufa.cas.cz)

J. C. Kasper and A. J. Lazarus, Kavli Institute for Astrophysics and Space Research, Massachusetts Institute of Technology, 77 Massachusetts Avenue, Cambridge, MA 02139, USA. (jck@mit.edu; ajl@space.mit.edu)